DMS gas transfer coefficients from algal blooms in the Southern Ocean

T. G. Bell[1,2*], W. De Bruyn[3], C.A. Marandino[4], S.D. Miller[5], C.S. Law[6,7], M.J. Smith[6] and E.S. Saltzman[2]

[1] Plymouth Marine Laboratory, Prospect Place, The Hoe, Plymouth, PL1 3DH, UK

[2] Department of Earth System Science, University of California, Irvine, CA, USA

[3] School of Earth and Environmental Science, Chapman University, Orange, California, CA, USA

[4] Forschungsbereich Marine Biogeochemie, GEOMAR / Helmholtz-Zentrum für Ozeanforschung Kiel, Düsternbrooker Weg 20, 24105 Kiel, Germany

[5] Atmospheric Sciences Research Center, State University of New York at Albany, NY, USA

[6] National Institute of Water and Atmospheric Research (NIWA), Evans Bay Parade, Kilbirnie Wellington, 6002, New Zealand

[7] Department of Chemistry, University of Otago, Dunedin, New Zealand

*Correspondence to: T.G. Bell (tbe@pml.ac.uk)

Abstract

Air/sea dimethylsulfide (DMS) fluxes and bulk air/sea gradients were measured over the Southern Ocean in February/March 2012 during the Surface Ocean Aerosol Production (SOAP) study. The cruise encountered three distinct phytoplankton bloom regions, consisting of two blooms with moderate DMS levels, and a high biomass, dinoflagellate-dominated bloom with high seawater DMS levels (>15 nM). Gas transfer coefficients were considerably scattered at wind speeds above 5 m/s. Bin averaging the data resulted in a linear relationship between wind speed and mean gas transfer velocity consistent with that previously observed. However, the wind speed-binned gas transfer data distribution at all wind speeds is positively skewed. The flux and seawater DMS distributions were also positively skewed, which suggests that eddy covariance-derived gas transfer velocities are consistently influenced by

27 additional, log-normal noise. A flux footprint analysis was conducted during a transect into the

28 prevailing wind and through elevated DMS levels in the dinoflagellate bloom. Accounting for the

29 temporal/spatial separation between flux and seawater concentration significantly reduces the scatter in

30 computed transfer velocity. The SOAP gas transfer velocity data shows no obvious modification of the

31 gas transfer-wind speed relationship by biological activity or waves. This study highlights the

32 challenges associated with eddy covariance gas transfer measurements in biologically active and

33 heterogeneous bloom environments.

34

1   Introduction

36 Gas exchange across the ocean-atmosphere interface influences the atmospheric abundance of many

37 compounds of importance to climate and air quality.   Such compounds include greenhouse gases,

38 aerosol precursors, stratospheric ozone-depleting substances, and a wide range of photochemically

39 reactive volatile organic carbon compounds that influence tropospheric ozone. Estimating the air/sea

40 fluxes of all of these compounds requires knowledge of their distributions in near surface air and

41 seawater and an understanding of the transport processes controlling gas exchange across the air/sea

42 interface. The transport processes are not well understood, in large part because of the paucity of direct

43 air/sea gas flux observations. The parameterization of gas exchange is a significant source of

44 uncertainty in ocean/atmosphere exchange in global models, particularly at high wind speeds (Elliott,

45 2009).

46 Gas flux is typically calculated using the concentration gradient across the air/sea interface (ΔC) and the

47 gas transfer coefficient (K):

$$Flux = K.\Delta C \qquad \qquad \text{Eqn. 1}$$

49 K represents the inverse of the resistance to gas transfer on both the water and air sides of the interface

50 (i.e. $1/K = r_w + r_a$) and can be expressed in either waterside or airside units (Liss and Slater, 1974).

51 Equation 1 is a very simple expression that belies the complex physical process involving diffusive and

52 turbulent mixing at the boundary between two mediums of very different densities. Wind stress is the

53 predominant forcing for gas transfer, but mixing at the interface is also influenced by buoyancy, wind-

54 wave interactions, wave breaking, surfactants, and bubble generation. The interface is chemically

2

55   complex owing to the presence of organic films or particles, and for some gases the interface may be

56   biologically/photochemically reactive.

57   Most air/sea gas transfer calculations utilize wind speed-based parameterizations derived from deliberate

58   dual tracer observations (Ho et al., 2011; Nightingale et al., 2000), sometimes scaled to agree with the

59   long-term global average oceanic uptake of $^{14}CO_2$ (Sweeney et al., 2007). The dual tracer technique is a

60   waterside method that requires data averaging over periods of hours to days, thus averaging over

61   significant changes in conditions. Eddy covariance is a direct flux measurement carried out on the air

62   side of the interface. In conjunction with measurements of the air/sea concentration difference, eddy

63   covariance studies can determine the gas transfer coefficient, K, on short time scales (10 minutes-1

64   hour). This provides a capability to assess variability in K due to the influence of rapid changes in near

65   surface processes (e.g. wind-wave interactions, bubbles, surfactants). Eddy covariance requires high

66   frequency sensors, and flux studies to date have been carried out on only a few compounds: DMS, CO_2,

67   methanol, acetaldehyde, acetone, ozone, carbon monoxide, dinitrogen pentoxide, chloro(oxo)azane

68   oxide and glyoxal (Huebert et al., 2004; McGillis et al., 2001; Yang et al., 2013; Kim et al., 2014;

69   Blomquist et al., 2012; Bariteau et al., 2010; Marandino et al., 2005; Coburn et al., 2014).

70   DMS air/sea transfer resistance is predominantly on the water side, a characteristic it shares with CO_2.

71   DMS is moderately soluble and weakly influenced by bubble-mediated gas transfer, in contrast to CO_2,

72   which is sparingly soluble and strongly influenced by bubble-mediated gas transfer. This makes DMS a

73   useful tracer for waterside-controlled, interfacial gas transfer. Measurements of gas exchange using

74   insoluble gases have suggested that the relationship between K and wind speed is non-linear

75   (Nightingale et al., 2000; Sweeney et al., 2007; Miller et al., 2010; Ho et al., 2011). In contrast, the

76   majority of DMS eddy covariance data suggests a linear relationship between K and wind speed (Yang

77   et al., 2011). Blomquist et al. (2006) suggest that the differences in functional form of these

78   relationships may be due to the disproportionate influence of bubbles upon the flux of insoluble gases

79   (Woolf, 1997).

80   Physical process models have made significant progress in parameterizing gas exchange with input

81   terms that include but are not limited to wind speed. However, these models are still in development

82   and are capable of substantially different estimates of K depending on how non-wind speed terms such

83   as wind-wave dynamics are applied in the model (Fairall et al., 2011; Soloviev, 2007). Bell et al. (2013)

84   recently demonstrated that some of the scatter in eddy covariance measurements may be explained by

85 spatial/temporal differences in wind-wave interaction, although the role of surfactants cannot be ruled
86 out. Gas exchange measurements in an artificial surfactant patch (Salter et al., 2011) and in laboratory
87 studies using natural surfactants (Frew et al., 1990) have demonstrated marked suppression of gas
88 transfer. Additional eddy covariance gas exchange observations are required to improve these gas
89 exchange models. Eddy covariance DMS flux measurements have been made in the Atlantic Ocean
90 (Bell et al., 2013; Marandino et al., 2008; Salter et al., 2011; Blomquist et al., 2006) and Pacific Ocean
91 (Marandino et al., 2007, 2009; Yang et al., 2009), with three of these studies at high northern latitudes.
92 Only one previous study has been performed in the Southern Ocean (Yang et al., 2011).

93 The Southern Ocean has a unique wind and wave environment: minimal land mass in the Southern
94 Hemisphere leads to strong, consistent winds and waves with a long fetch. The duration of the wind
95 speed event rather than the wind fetch is the most important factor influencing the waves (Smith et al.,
96 2011). This region is very important in determining the global uptake of atmospheric CO_2 by the ocean
97 (Sabine et al., 2004) and the supply of DMS as a source of atmospheric sulfate aerosol (Lana et al.,
98 2011). This paper presents data collected in the Southern Ocean summer (Feb-March 2012) as part of
99 the New Zealand Surface Ocean Aerosol Production (SOAP) cruise (Figure 1). During the cruise, a
100 variety of oceanic, atmospheric and flux measurements were collected. The cruise targeted regions of
101 extremely high biological activity (blooms of dinoflagellates and coccolithophores) and encountered a
102 number of atmospheric frontal events leading to winds in excess of 11 m/s.
103
104 **2   Methods**

105 **2.1 Mast-mounted instrumentation and data acquisition setup**

106 The eddy covariance setup was mounted on the bow mast of the *R/V* Tangaroa, 12.6 m above the sea
107 surface. Three dimensional winds and sonic temperature (Campbell CSAT3) and platform angular rates
108 and accelerations (Systron Donner Motion Pak II) were measured on the mast and co-located with the
109 air sampling inlets for DMS. Air was drawn through the sampling inlets at 90 SLPM under fully
110 turbulent flow conditions ($Re > 10,000$). Analog signals from all of these instruments were filtered at 15
111 Hz and then logged at 50 Hz (National Instruments SCXI-1143). The ship's compass and GPS systems
112 were digitally logged at 1 Hz. The mast configuration was similar to that used during the Knorr_11
113 North Atlantic cruise (Bell et al., 2013), with the following two changes:

114   1) An air sampling inlet with integral ports for standard delivery was fabricated from a solid block of

115   PTFE. The design minimized regions of dead space that might attenuate high frequency fluctuations

116   and result in loss of flux signal.

117   2) A shorter length of ⅜″ ID Teflon tubing was used between the mast and the container van. A 19 m

118   inlet was used during SOAP in contrast to the 28 m inlet used during Knorr_11 (Bell et al., 2013).

119

2.2 Atmospheric and seawater DMS

121   DMS was measured in air and in gas equilibrated with seawater using two atmospheric pressure

122   chemical ionization mass spectrometers (Bell et al., 2013). In both instruments, a heated (400°C)

123   radioactive nickel foil (Ni-63) generates protons that associate with water molecule clusters in the

124   sample stream. Protonated water vapor (H_3O^+) undergoes a charge transfer reaction to form protonated

125   DMS ions (m/z=63) that are then quadrupole mass filtered and counted. Tri-deuterated DMS (d3-DMS,

126   m/z=66) was used as an internal standard for both instruments.

127   Atmospheric measurements were made with the University of California, Irvine (UCI) mesoCIMS

128   instrument (Bell et al., 2013). A gaseous d3-DMS standard was introduced to the atmospheric sample

129   stream at the air inlet via a 3-way valve mounted at the base of the bow mast. The gas standard was

130   diverted to waste every 4 hours and the response of the d3-DMS signal recorded as a measure of the

131   inlet tubing impact on signal delay and frequency loss. Air from the bow mast was sub-sampled at

132   approximately 1 L min⁻¹ and DMS levels were calculated as follows:

$$DMS_a = \frac{S_{63}}{S_{66}} \cdot \frac{F_{Std}}{F_{Total}} \cdot C_{Tank}$$ Eqn. 2

134   Where S_{63} and S_{66} represent blank-corrected signals from DMS and d3-DMS respectively (Hz), F_{Std} and

135   F_{Total} are the gas flow rates of the d3-DMS standard and the inlet air (L min⁻¹), and C_{Tank} is the gas

136   standard mixing ratio.

137   Seawater measurements were made with a smaller instrument (UCI miniCIMS), which utilizes a

138   modified residual gas analyzer as the mass filter and ion detector (Stanford Research Systems RGA-

139   200; Saltzman et al. (2009)). Aqueous d3-DMS standard was delivered by a syringe pump (New-Era

140   NE300) to the ship's underway seawater supply upstream of the equilibrator (see Bell et al., 2013, for

141   details). The natural DMS and the d3-DMS standard are both transported across the membrane and the

142   DMS concentration in seawater in the equilibrator is then calculated as follows:

143    $$DMS_{SW} = \frac{Sig_{63}}{Sig_{66}} \cdot \frac{F_{Syr}}{F_{sw}} \cdot C_{Std}$$ Eqn. 3

144   Sig_{63} and Sig_{66} represent the average blank-corrected ion currents (pA) of protonated DMS (m/z=63) and

145   d3-DMS (m/z=66), respectively, C_{Std} is the concentration of d3-DMS liquid standard (nM), F_{Syr} is the

146   syringe pump flow rate (L min^{-1}), and F_{sw} is the seawater flow rate (L min^{-1}). Seawater concentrations

147   were averaged at 1 minute intervals for the entire SOAP dataset. Lag correlation analysis between the

148   ship surface seawater temperature and equilibrator temperature records identified that a 3-4 minute

149   adjustment in the DMS_{sw} was required to account for the delay between water entering the seawater

150   intake beneath the hull of the ship and it reaching the miniCIMS equilibrator.

151   We compared our seawater measurements with discrete samples collected by the NIWA team and

152   analysed using sulfur chemiluminescence detection (SCD). The NIWA discrete analyses were

153   performed on water collected from both the underway supply and from CTD Niskin bottles fired in the

154   near surface (<10 m). The analytical techniques (SCD and miniCIMS) typically agreed well and these

155   results will be discussed elsewhere. Throughout the cruise, data from the underway and CTD bottles

156   were in good agreement (Figure 2), with the exception of Day of Year (DOY) 54-55 when the ship's

157   underway supply became significantly contaminated. The contamination was biological and resulted in

158   DMS levels at least twofold higher than from a Niskin bottle fired at the same depth. Flushing and

159   soaking the underway lines in a biologically-active cleaning solution (Gamazyme[TM]) and cleaning the

160   equilibrator with dilute (10 %) hydrochloric acid resolved the problem. The data from DOY 54-55 has

161   been excluded from our analysis.

162   ## 2.3 DMS flux calculation: eddy covariance data processing and quality control

163   Air/sea flux calculation involved the same procedure detailed in Bell et al. (2013). Apparent winds were

164   corrected for ship motion according to the procedures of Edson et al. (1998) and Miller et al. (2008).

165   Relative wind speed was adjusted to correct for air-flow distortion according to the wind direction-

166   dependent correction presented by Smith et al. (2011), which uses the computational fluid dynamics

167   Gerris model (Popinet et al., 2004). Ten minute flux intervals with a mean relative wind direction

168   within ±90° (where winds onto the bow = 0°) were retained for subsequent data analysis. The DMS

169 signal was adjusted relative to the wind signals to account for the timing delay due to the inlet tubing.

170 The delay was estimated to be 1.9 seconds from the periodic firing of a 3-way valve on the bow mast.

171 An equivalent delay estimate was ascertained by optimization of the cross correlation between DMS and

172 vertical wind. Flux intervals were computed from the co-variation in fluctuations in vertical winds (w')

173 and DMS (c') flux. The internal d3-DMS standard exhibited negligible covariance with vertical wind,

174 confirming that no density correction due to water vapor or temperature fluctuations (i.e. 'Webb'

175 correction) was required for our DMS fluxes.

176 Cospectral analysis objectively removed intervals with large low frequency fluctuations and the criteria

177 for elimination is defined in Bell et al. (2013). This process reduced scatter in the data without

178 introducing an obvious bias. High frequency flux loss in the inlet tubing was estimated by modeling a

179 filter based on the d3-DMS signal attenuation when the bow mast valve was switched. The inverse filter

180 was then applied to wind speed binned DMS cospectra. This enabled an estimate of the necessary wind

181 speed-dependent high frequency loss correction (Flux Gain = $0.004U_{10n}$ + 1.012).

182 ### 2.4 DMS gas transfer velocity calculation

183 Gas transfer velocities were calculated following:

184
$$K_{DMS} = \frac{F_{DMS}}{\Delta C} = \frac{F_{DMS}}{DMS_{sw} - \left(DMS_{air}/H_{DMS}\right)}$$
Eqn. 4

185 Where F_{DMS} is the measured DMS air/sea flux (mol m^{-2} s^{-1}), DMS_{sw} is the seawater DMS level (mol m^{-3}

186 ^{3}), DMS_{air} is the atmospheric DMS partial pressure (atm), and H_{DMS} is the temperature-dependent DMS

187 solubility in seawater (atm m^{3} mol^{-1}; Dacey et al. (1984)). K_{DMS} values were calculated from the cruise

188 data using 10 minute averages.

189 The water side only gas transfer coefficient, k_w, was obtained from the expression:

190
$$k_w = \left[\frac{1}{K_{DMS}} - \frac{1}{\alpha.k_a} \right]^{-1}$$
Eqn. 5

191 Where K_{DMS} is the total DMS gas transfer coefficient, α is the dimensionless Henry's Law constant for

192 DMS, and k_a is the air side gas transfer coefficient. *In situ* k_a values were obtained from NOAA

193 COARE driven by *in situ* measurements of wind speed, atmospheric pressure, humidity, irradiance and

194 air and seawater temperature. The relative influence of k_a upon our estimates of k_w was greater when

195   measured K_{DMS} was high (Figure A, Supplemental material). This has little impact upon our data as the

196   average (mean) difference between k_w and K_{DMS} was 7% and showed no wind speed dependence (Figure

197   B, Supplemental material). In order to compare our results with various other gas transfer

198   parameterizations, k_w was then normalized to a Schmidt number of 660 (CO_2 at 25°C):

199
$$k_{660} = k_w \cdot \left(\frac{660}{Sc_{DMS}} \right)^{-\frac{1}{2}}$$
Eqn. 6

200   Where Sc_{DMS} is calculated using the ship's seawater temperature recorded at the bow and Eqn. 15 in

201   Saltzman et al. (1993).

202

203   **3   Results**

204   **3.1 Cruise track, meteorological, and oceanographic setting**

205   The SOAP cruise sampling strategy was to identify phytoplankton blooms using ocean color imagery

206   and then use underway sensors (e.g. chlorophyll *a* fluorescence, DMS) to map out the *in situ* spatial

207   distribution. Three blooms were identified and sampled: *B1*, *B2* and *B3* (Figure 1). *B1* was an intense

208   dinoflagellate-dominated bloom at approx. 44.5°S, 174.7°E (DOY 45.9-49.8) with extremely high levels

209   of seawater DMS (16.8±1.5 nM). After *B1* the ship headed south-west to a waypoint (*WP1*) at approx.

210   46.3°S, 172.5°E (DOY 50.5). The waters at *WP1* contained moderate DMS signals (3.8±0.4 nM) and

211   weakening fluorescence (0.83±0.38 mg/m^3) so minimal time was spent at this location.   The return

212   transect into *B1* from *WP1* is discussed in detail in Section 3.3. The second bloom (*B2*) was a

213   coccolithophore-dominated bloom at approx. 43.6°S, 180.2°E (DOY 52.9–56.1) that had stronger DMS

214   signals (9.1±2.9 nM) and fluorescence (0.99±0.35 mg/m^3). After sampling *B2*, the *B1* location was

215   revisited and a new bloom (*B3*) was identified with a mixed population of coccolithophores, flagellates

216   and dinoflagellates (DOY 57.9–60.5). *B3* DMS levels (5.9±1.5 nM) were substantially lower than in

217   *B1*.

218
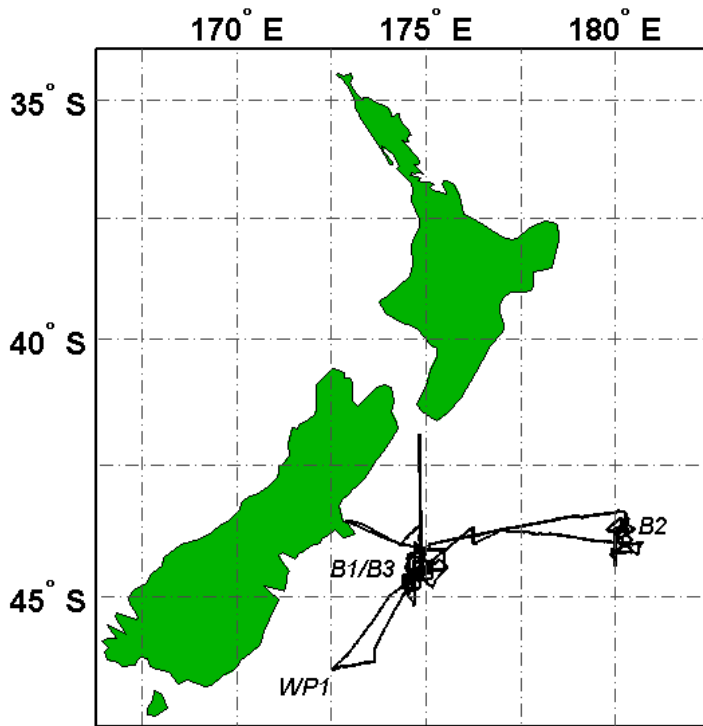
Figure 1
Cruise track during the SOAP study, which began and finished in Wellington, New Zealand. The
phytoplankton blooms (*B1-3*) and waypoint 1 (*WP1*) locations are identified.

The time series plot in Figure 2 describes the oceanographic and meteorological variability throughout

the cruise. Surface ocean temperatures (SSTs) were consistent at 14.7±1.0°C while atmospheric

temperature fluctuated just above and below the SST. Weather systems from the North brought

relatively warm air and systems from the South brought cooler air. For example, the atmospheric front

on DOY 55 from the South caused air temperatures to drop from approximately 18°C to 12°C (Figure

2a). Frontal systems passed over the ship regularly throughout the cruise and the final system (DOY

61.6 –64) brought intense winds from the North. During SOAP, the horizontal wind speeds

predominantly ranged between 1 and 15 m/s. The atmospheric boundary layer was stable ($z/L > 0.05$)

for approximately 25% of the cruise (Figure 2a). Yang et al. (2011) suggest that a stable boundary layer

leads to greater scatter and a potentially negative bias in k_{660} vs. wind speed plots. Our data do not

suggest increased scatter or any bias during stable periods (Figure C, Supplemental material) and we

have not filtered the SOAP k_{660} data on this basis.

Oceanic and atmospheric DMS levels were extremely high during the first half of the cruise (DOY 44–

54; Figure 2c). The majority of this period was spent in and around *B1* waters, with elevated seawater

9

237 DMS (> 10 nM) and atmospheric DMS (> 600 ppt). Oceanic DMS was always at least an order of

238 magnitude greater than atmospheric DMS, meaning that the air/sea concentration gradient was

239 effectively controlled by DMS_{sw}. The second half of the cruise (DOY 55–65) encountered less

240 productive blooms with lower seawater DMS levels. The reduction in oceanic DMS was mirrored by

241 lower atmospheric DMS levels (151±73 ppt, DOY 55–65).

242 Ten minute average DMS fluxes (F_{DMS}) measured by eddy covariance are plotted in Figure 2. F_{DMS}

243 reflected the seawater DMS levels, with three notable peaks while inside $B1$ waters (> 60 µmol m^{-2} day^{-}

244 ^{1}, DOY 48–50). F_{DMS} was generally lower during the second half of the cruise (13±10 µmol m^{-2} day^{-1},

245 DOY 55–65) but elevated fluxes were still observed due to increased horizontal wind speeds (e.g.

246 approx. 45 µmol m^{-2} day^{-1} on DOY 61.6). SOAP gas transfer coefficients were calculated at 10 minute

247 intervals (Figure 2e) following Eqns. 1-6 using measurements of F_{DMS}, oceanic and atmospheric DMS

248 levels and SST. During some periods of constant wind speed, the NOAA COARE (v3.1) estimates are

249 close to the observed k_{660} values (e.g. DOY 51).   However, at various times during the cruise, the

250 NOAA COARE estimates exhibit significant divergence from the observed k_{660} values. The difference

251 was sometimes positive, as on DOY 48 and sometimes negative, as on DOY 53. These divergences are

252 not random scatter about the COARE prediction and suggest that unaccounted-for processes are

253 influencing our measurements of gas transfer.
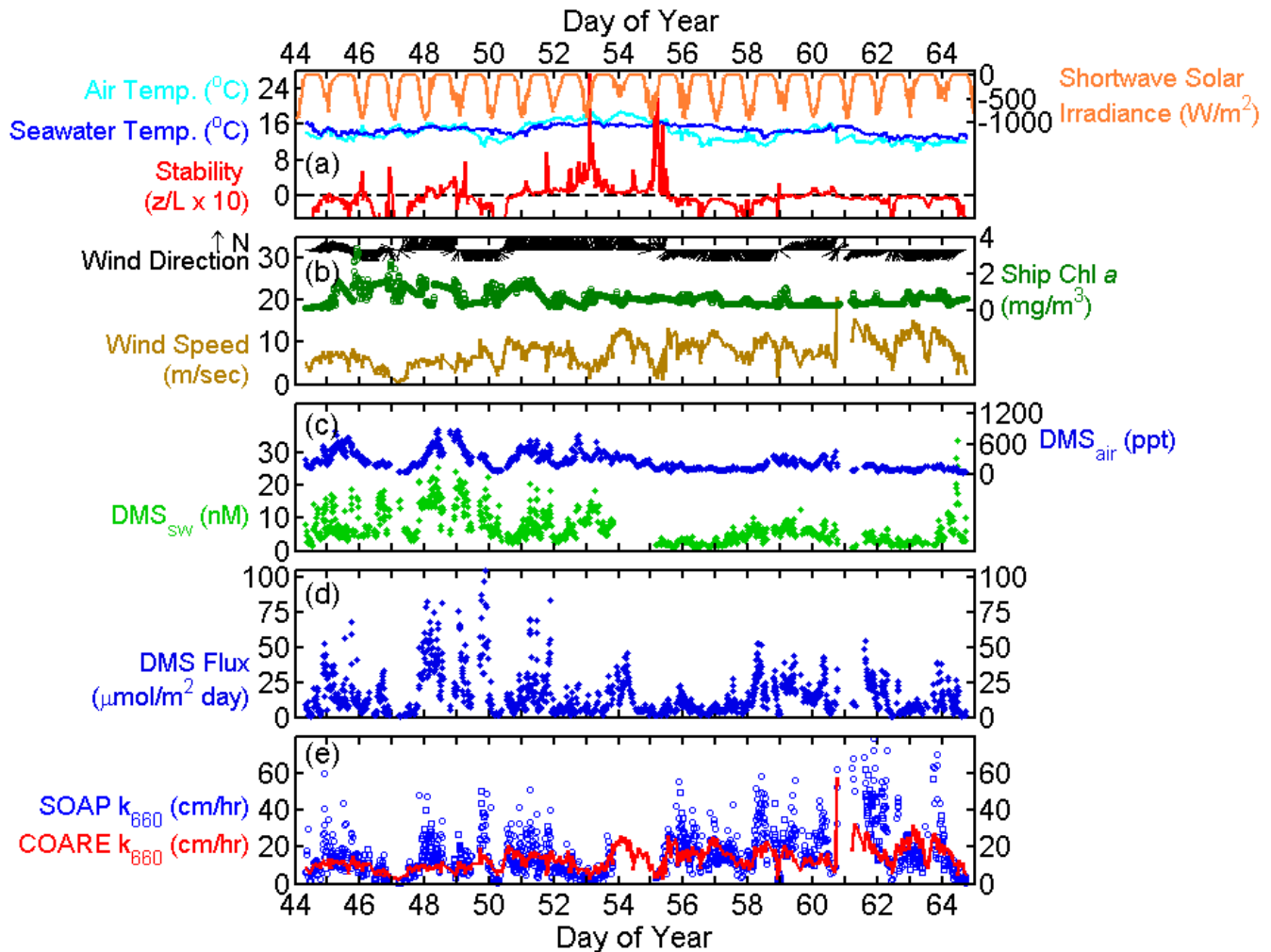
254
255 **Figure 2**
256 Time series data (10 min averages) from the SOAP cruise. Dashed black line on (a) indicates neutral
257 atmospheric stability (z/L=0). SOAP k_{660} data (e) are divided into on station (squares, ship speed < 1.5
258 m/s) and off station (circles, ship speed ≥ 1.5 m/s).
259

3.2 Wind speed dependence of gas transfer coefficients

261 The SOAP gas transfer coefficients exhibit a positive correlation with wind speed (Spearman's ρ = 0.57,

262 $p<0.01$, $n=1327$; Figure 3a). A linear least squares fit to the data gives $k_{660}=2.31\pm0.11U_{10n} - 1.51\pm0.97$

263 with an adjusted R^2=0.25. As with previous shipboard eddy covariance DMS studies, using a second

264 order polynomial does not improve the fit to the data (adjusted R^2=0.25). The linear model is not well

265 suited for this data set because the residuals are not normally distributed (Figure 3b). The frequency

266 distribution of the SOAP k_{660} measurements exhibits positive skewness at all wind speeds (Figure D,

267 Supplemental material). The skew in the SOAP k_{660} data appears to originate in the frequency

268 distribution of seawater DMS. Surface ocean DMS distributions are typically characterized by positive

269 skew and this is evident in the global surface ocean DMS database (Lana et al., 2011).

270
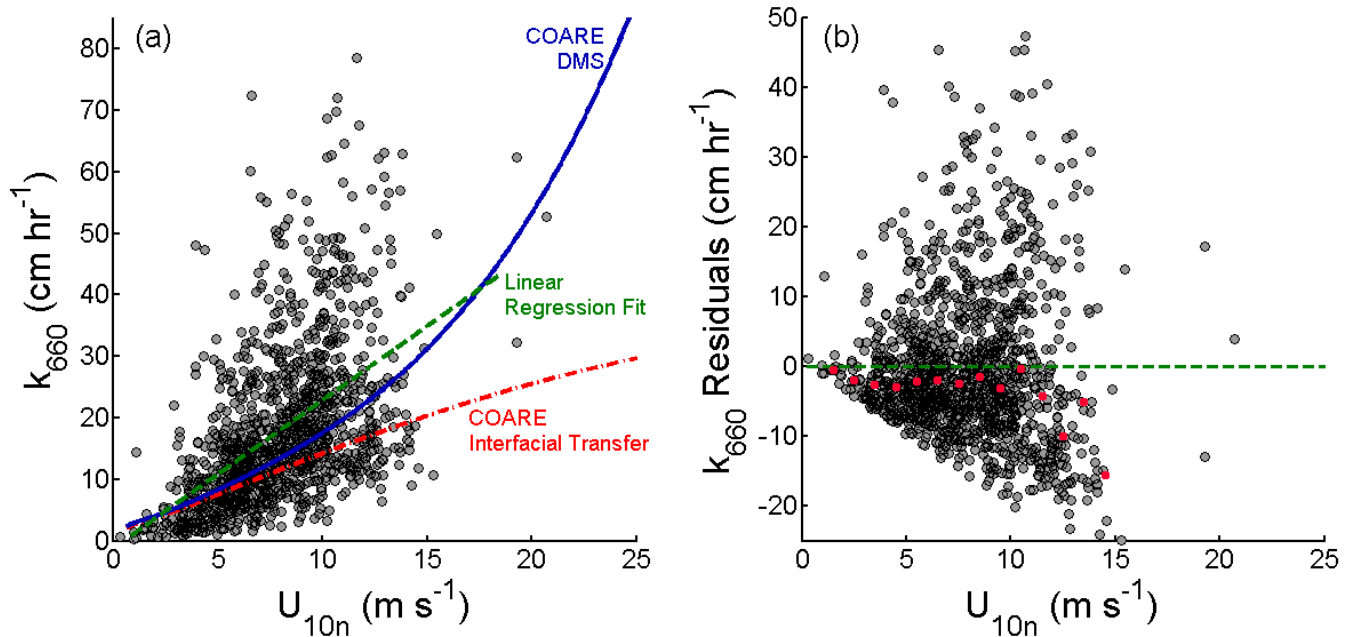
Figure 3
271
272 (a) 10 minute average DMS gas transfer coefficients vs. mean horizontal wind speed during the SOAP
273 cruise, expressed as k_{660} and U_{10n} (see Methods). For reference the NOAA COARE model output for
274 DMS is plotted, calculated using average SOAP input parameters and the turbulent/molecular
275 coefficient, $A=1.6$, and the bubble-mediated coefficient, $B=1.8$. Red dashed line is interfacial transfer
276 velocity only. Blue solid line includes the bubble contribution to gas transfer. Green dashed line is least
277 squares linear regression fit to the SOAP 10 min averaged data ($k_{660} = 2.31U_{10n} - 1.51$). (b) Residual
278 values from the least squares linear regression fit in (a). Green dashed line is exact agreement with
279 linear regression model. Red squares are the median residual within each 1 m/s wind speed bin.
280 Negative deviation of the median residuals from the linear regression demonstrates the positive skew in
281 k_{660}.
282

283 It is not surprising to see skewed distributions in the SOAP data as the cruise encountered strong, non-

284 linear gradients in biological activity. There is no skewness in the distribution of winds within each

285 wind speed bin. Skewness in the seawater DMS distribution should propagate into the DMS flux

286 distribution simply because air/sea flux is proportional to air/sea concentration gradient, which is

287 controlled in turn by seawater DMS levels (Figures E&F, Supplemental material). If F_{DMS} and ΔC are

288 highly correlated, then the variance in k_{660} should be considerably less than that in either parameter and

289 would exhibit less skew. This is not the case: k_{660} exhibits a similar skew to F_{DMS} and ΔC. For

290 example, the correlation coefficient between DMS flux and seawater concentration in the 13-14 m/s

291 wind speed bin (Spearman's $\rho = 0.45$, $p<0.01$, $n=47$) is considerably lower than expected. Decorrelation

292   of DMS flux and seawater concentration is likely due to mismatches between seawater DMS levels

293   measured aboard ship and those in the actual footprint of the flux. Misalignment between seawater

294   DMS levels and the flux footprint is virtually unavoidable in a region of strong spatial heterogeneity,

295   where wind direction and ship track are never perfectly aligned.

296   As a result of the frequency distribution observations in the SOAP dataset, we reexamined data from a

297   recent North Atlantic cruise (Bell et al., 2013; Figures E-G, Supplemental material).   The frequency

298   distributions of k_{660}, F_{DMS} and DMS_{sw} exhibit similar positive skewness to that in the SOAP data set. In

299   order to better represent the central tendency of the k_{660} data and assess the relationship with wind speed,

300   geometric means were computed for 1 m/s wind speed bins (Figure 4). Geometric binned k_{660} data from

301   both cruises are lower than the arithmetic binned data. The binned k_{660} SOAP data demonstrate a

302   shallower slope using the geometric means.

303

304
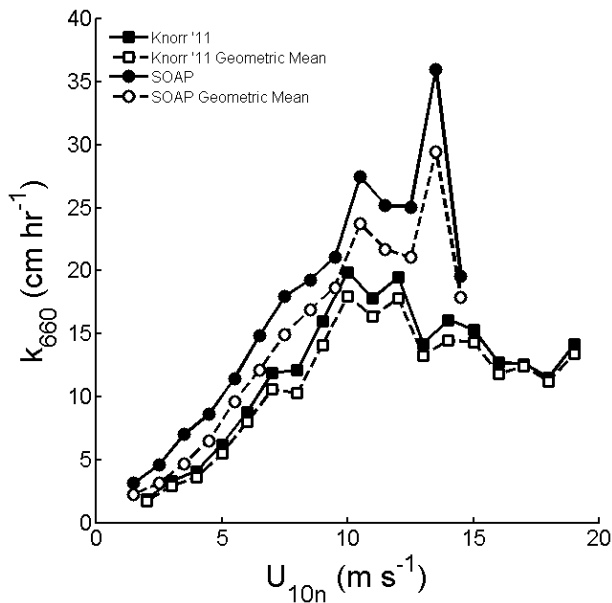
Figure 4: Bin average gas transfer coefficients for this study (SOAP) and the data collected in the
North Atlantic (Knorr '11). Mean values were calculated for 1 m/s U_{10n} bins using arithmetic (solid
lines, filled symbols) and geometric (dashed lines, open symbols) approaches.

308

309   The SOAP k_{660} bin average data (Figure 5) exhibit a linear relationship with wind speed for low and

310   intermediate winds, as found in previous DMS flux studies (e.g. Huebert et al., 2010; Yang et al., 2011;

311   Marandino et al., 2007, 2009). For wind speeds up to 14 m/s, the binned geometric mean SOAP data

312   yields a linear regression equation of $k_{660} = 2.07U_{10n} - 2.42$, which is slightly shallower than that

313   obtained from a compilation of previously published DMS gas transfer measurements ($k_{660} = 2.6U_{10n} -$

314   5.7; Goddijn-Murphy et al., 2012). In the higher wind speed bins (above 10 m/s), the relationship

315   between k_{660} and wind appears to weaken. A weaker relationship between k_{660} and wind speed at high

316   wind speeds was also observed in the North Atlantic (Bell et al., 2013). In both cruises, there is limited

317   data at wind speeds above 10 m/s, so this phenomenon should be viewed with caution. Bell et al. (2013)

318   suggested that the effect could be due to suppression of near surface waterside turbulence due to

319   wind/wave interactions (Soloviev et al., 2007; Donelan et al., 2010).
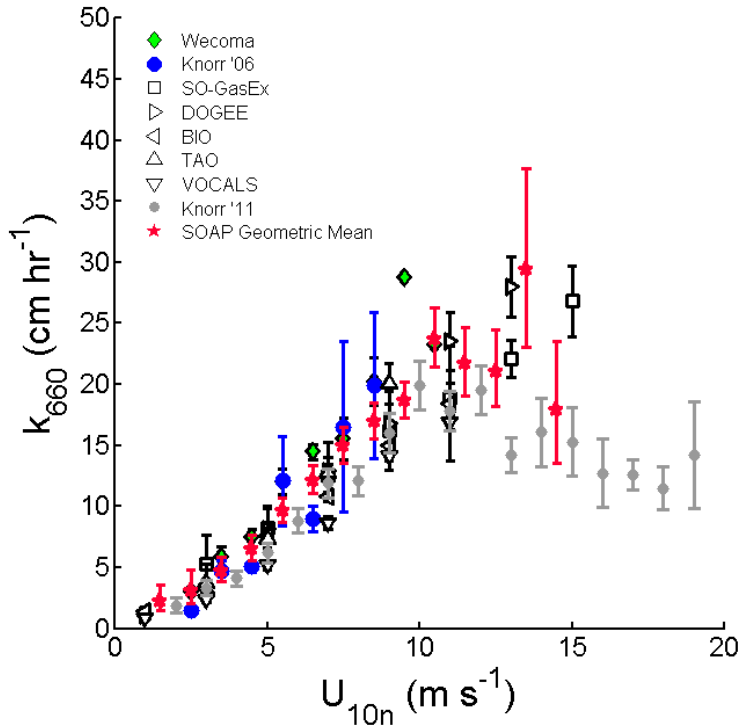
320
321   **Figure 5:** Bin average gas transfer coefficients from this study compared with prior published DMS
322   eddy covariance measurements: Wecoma (Marandino et al., 2007), Knorr '06 (Marandino et al., 2009),
323   SO-GasEx (Yang et al., 2011), DOGEE (Huebert et al., 2010), BIO (Blomquist et al., 2006), TAO
324   (Huebert et al., 2004), VOCALS (Yang et al., 2011) and Knorr '11 (Bell et al., 2013). Geometric mean
325   SOAP k_{660} values were calculated for 1 m/s U_{10n} bins (error bars represent ± 2 SE; minimum data points
326   per interval = 6).

327

328   The SOAP study did not include direct measurements of wave properties or surfactants. Significant

329   wave height was estimated using satellite reanalysis products from ECMWF and NCEP, which agreed

330   well (Spearman's $\rho = 0.91$, $p<0.01$, $n=2876$). Significant wave height exceeded 4.5 m during SOAP.

331   There is no obvious relationship between significant wave height and the scatter in the relationship

332   between gas transfer and horizontal wind speed during SOAP (Figure J, Supplemental material). *In situ*

333   fluorescence was used as an indicator of biological activity during SOAP. Fluorescence sensors were

334   located in seawater continuously pumped through the ship from the near surface intake beneath the hull.

335   The variability in the gas transfer velocity data is not explained by surface ocean fluorescence (Figure K,

336   Supplemental material). Note that fluorescence is not necessarily a reliable indicator of surfactant

337   concentrations. The relative importance of waves and/or surfactants in air/sea gas exchange remains

338   unclear and requires dedicated measurements to be made concurrent with direct assessments of gas

339   exchange by eddy covariance.

340   ## 3.3 Uncertainties in *K* introduced by flux footprint and seawater DMS heterogeneity

341   As discussed above, spatial heterogeneity of seawater DMS can introduce uncertainty in gas transfer

342   coefficients derived from eddy covariance studies. It is logistically challenging to quantify footprint

343   effects from a single ship, and it has not been done on prior studies. On the SOAP cruise, the fortuitous

344   alignment of winds and ship track downwind of the dinoflagellate-dominated bloom (*B1*) provided a

345   unique opportunity to quantify the length scale associated with the flux footprint.
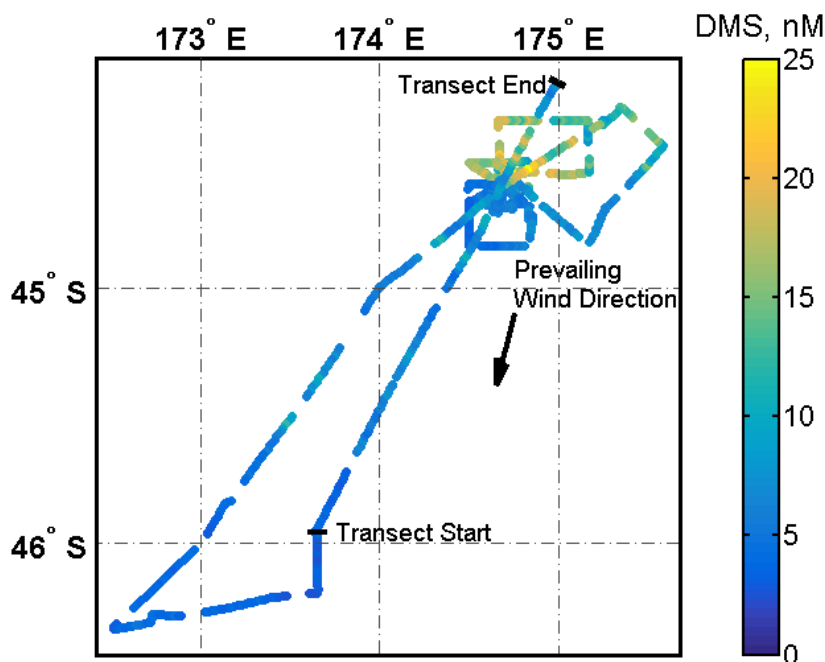
346
347   **Figure 6:** Latitude-longitude map of surface ocean DMS concentrations (nM) in and around *B1* waters
348   between DOY 45.65 and 51.35. Start and End points of the transect into *B1* are indicated. Arrow
349   indicates prevailing wind direction along the transect.

350

351 The SOAP cruise spent approximately 5 days mapping out the spatial extent of *B1* waters, then transited

352 out of the bloom to *WP1* about 150 km to the southwest. The ship then steamed back into and across

353 *B1* at a ship speed of 5.1±0.7 m/s, over about 18 hours (DOY 50.85–51.35; Figure 6). Meteorological

354 and oceanographic conditions were relatively constant during the *B1* transect, with wind speeds ranging

355 from 5.5-9.7 m/s, wind direction from 5-33°, air temperature of 15.4±0.8, and SST of 14.4±0.5 (Figure

356 7). Atmospheric stability was neutral-stable during this period. A detailed picture of surface ocean

357 DMS levels in and around *B1* can be seen from the data collected between DOY 45.65 and DOY 51.35

358 (Figure 6). DMS levels exhibit a sharp step-change at approximately 44.6°S. DMS concentrations

359 south of the bloom were less than 5 nM. Near the bloom center, levels increased rapidly over a few

360 kilometers from below 10 nM to greater than 15 nM. Atmospheric DMS levels were quite stable during

361 the transect with a mean of 489±58 ppt. The ship's heading (approx. 27°) meant that winds blew almost

362 directly onto the bow, with <10° difference for the final 60 km of the transect back into *B1*.
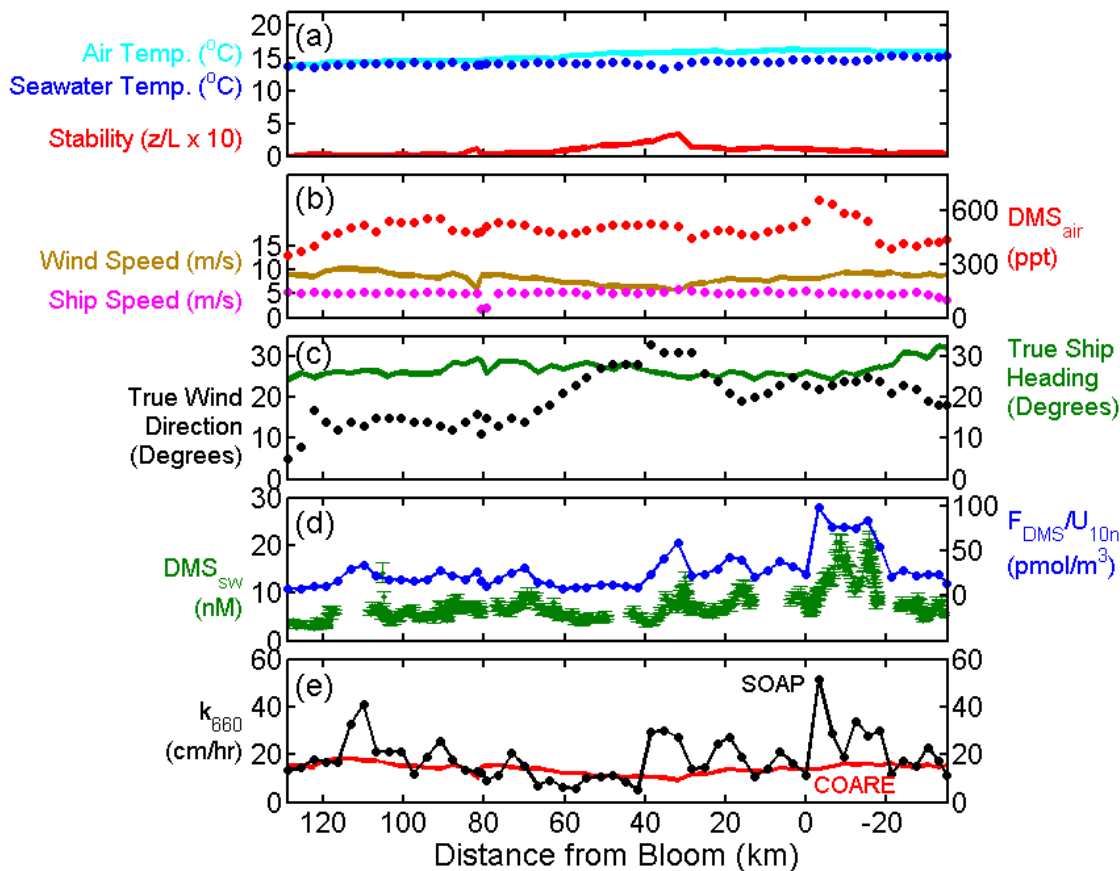
363
364 **Figure 7**
365 Shipboard measurements during the South-North transect into *B1*. The data are plotted as a function of
366 distance from the southern perimeter of the bloom. Symbols represent 10 minute averages, with the
367 exception of 1 min average seawater DMS concentrations (d). Red line in (e) is the COARE model
368 output for DMS, shown for reference.

16

369

Figure 7 depicts seawater DMS levels (green symbols) as the ship steamed into *B1* waters. DMS levels 120 km away from the bloom were below 5 nM and consistently 5-10 nM until the southern perimeter of the bloom (0 km). DMS levels increased rapidly to 15-20 nM as the ship moved into the bloom. DMS flux divided by the horizontal wind speed is also presented. We assume a relatively linear relationship between k_{660} and U_{10n} and that fluctuations in F_{DMS}/U_{10n} (Figure 7, blue symbols) are driven primarily by changes in ΔC (i.e. DMS_{sw}). Spikes in F_{DMS}/U_{10n} are evident in DMS_{sw} after a consistent distance/time lag. The gas transfer velocities are shown in Figure 7e during the transect into *B1*. COARE model output for DMS is plotted as a reference line. Spikes in k_{660} are coincident with sharp changes in F_{DMS}/U_{10n} prior to the lagged corresponding change in DMS_{sw}.

On this transect the eddy covariance flux footprint was directly ahead of the ship, so a lag would be expected between the F_{DMS} and ΔC *(i.e. DMS_{sw})*. The maximum correlation between F_{DMS}/U_{10n} (using the midpoint of the flux interval) and ΔC was obtained for a lag of 8 minutes. This lag represents a distance of ~2.5 km at 5.1m/s ship speed. Applying this lag to the calculation of gas transfer velocity reduced the scatter (Figure 8). We compared the flux footprint obtained from the lag calculation to a flux footprint calculation using an online version of an analytic dispersion model (http://www.geos.ed.ac.uk/abs/research/micromet/java/flux.html; Kormann & Meixner, 2001). We ran the model with representative conditions for the SOAP *B1* transect: measurement height = 12 m; wind speed = 8 m/s; roughness length = 0.02 m (minimum value available); zero-plane displacement = 0.5 m (minimum value available); sensible heat flux = -20 W/m^2; air temperature = 15°C. The footprint model predicts a peak relative flux contribution (defined as 90% of the relative flux) 0.8 km ahead of the ship, less than half of the distance inferred from the field observations. The calculated footprint is highly sensitive to the input parameters. During the SOAP *B1* transect, atmospheric stability was slightly stable but close to neutral (z/L ~ +0.1). Relatively small changes in wind speed (±1 m/s), temperature (±1°C) or sensible heat flux (+10 W/m^2) alter the stability such that model predictions of the peak footprint contribution range from 0.3 km to 1.9 km. Model runs where measurement height was varied to reflect the limits of ship motion (significant wave height from ECMWF suggests the vertical displacement of the flux inlet was at least 2.5 m) gave minimum and maximum peak flux footprint contributions of 0.4 and 2.0 km respectively.

398   Despite the sensitivity of the model to the input parameters, none of these estimates are as large as the

399   footprint derived from the lag calculation. Flux footprint models make the assumption that the surface

400   source is spatially homogeneous. This was not true during the SOAP *B1* transect – the location of the

401   peak contribution to the flux was not the same as the peak in the footprint model. Greater DMS_{sw}

402   concentrations at the furthest extent of the flux footprint will cause the flux signal to be dominated by a

403   signal from further afield than implied by the footprint model. This is the likely explanation for the

404   mismatch between our correlation analysis and the flux footprint model output.
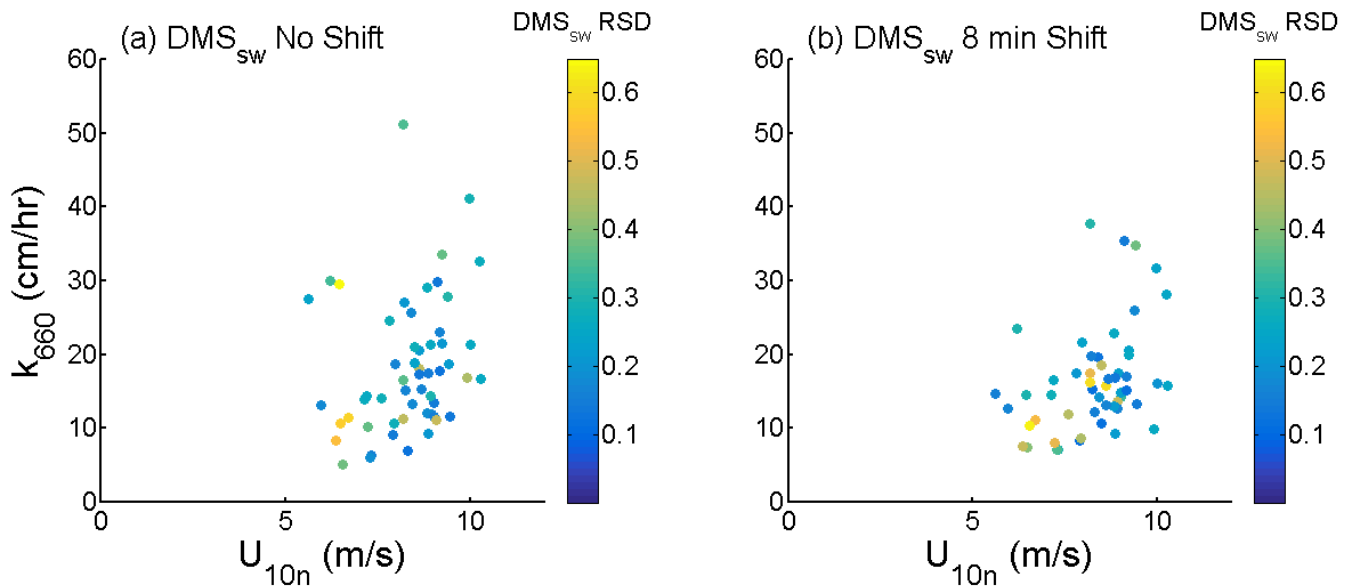
405

406   **Figure 8**
407   10 minute average DMS gas transfer coefficients (k_{660}) vs. mean horizontal wind speed (U_{10n}) during the
408   South-North transect into *B1* waters. Data are coloured by the relative standard deviation (RSD) for
409   corresponding DMS_{sw} (see text). (a) Gas transfer velocities calculated before adjustment of DMS_{sw} to
410   account for decoupling from the flux footprint. (b) k_{660} calculated using seawater DMS shifted by 8
411   minutes to account for the lag between measured flux and ΔC (see text).

412

413   Huebert et al. (2010) addressed surface ocean spatial heterogeneity for their estimates of DMS gas

414   transfer velocity during the June 2007 Deep Ocean Gas Exchange Experiment (DOGEE) in the North

415   Atlantic. When hourly DMS_{sw} relative standard error of the mean (RSEM) exceeded 0.25, gas exchange

416   data was not included in their analysis. Removing k_{660} data with high DMS_{sw} variability during DOGEE

417   improved the correlation between k_{660} and wind speed. We assessed variability in our high frequency

418   DMS_{sw} data by calculating the forward-looking, running standard deviation (SD) on a one hour

419   timescale. The relative standard deviation (RSD) was then calculated by dividing the SD by DMS_{sw}.

420   Using the RSD would not have been reliable for identifying the outlying k_{660} data during the *B1* transect

421   (Figure 8a). The scatter in k_{660} versus U_{10n} in the entire SOAP dataset cannot be reduced on the basis of

422   the associated RSD values (Figure L, Supplemental material).

423

4   Conclusions

425   The SOAP k_{660} bin average values are in good agreement with previous gas transfer studies using eddy

426   covariance of DMS (Yang et al., 2011; Bell et al., 2013; Marandino et al., 2007). As noted earlier, these

427   studies provide evidence that interfacial gas transfer is a relatively linear function of wind speed for low-

428   intermediate wind speeds. There is some evidence that the dependence on wind speed weakens at

429   higher wind speeds both in this study and in the Knorr_11 study (Bell et al., 2013). There is no evidence

430   in any of the DMS eddy covariance data sets that the interfacial (non-bubble mediated) component of

431   gas transfer has a wind speed-dependence greater than linear. However there is still very limited data

432   above 10 m/s and the high wind speed trends are uncertain.

433   The scatter in the SOAP data is typical of shipboard eddy covariance flux measurements. This arises

434   from fluctuations in near surface turbulence and vertical entrainment, vertical shear, ship motion,

435   heterogeneity in seawater DMS and variations in atmospheric DMS due to chemical losses (Blomquist

436   et al., 2010). We note the skewness of the gas transfer velocities in a given wind speed range and use

437   geometric statistics to characterize the central tendency and variance of the data. This skewness is likely

438   driven by the inherent lognormal distribution of seawater DMS levels. We propose that spatial

439   heterogeneity in seawater DMS causes decorrelation between the measured seawater DMS and the

440   observed DMS flux, which results in skewness propagating into the calculated transfer coefficients. The

441   data from this study may be particularly influenced by the large differences in seawater DMS values

442   inside and outside the phytoplankton blooms. Similar skewness was observed in data from the North

443   Atlantic ocean (Bell et al., 2013) and this phenomenon likely affects all DMS eddy covariance studies to

444   some degree. If so, then some transformation of the DMS gas transfer velocities is warranted.

445   The transect from *WP1* into *B1* provided a unique opportunity to quantitatively estimate the spatial

446   extent of the eddy covariance flux footprint. The data suggest that the shipboard flux measurements

447   were sensitive to changes in seawater DMS approximately 2.5 km upwind of the ship, a surprisingly

448   large distance. This transect was conducted under neutral to stable conditions, when one might expect

449   the flux footprint to be relatively large. This result is much greater (twofold or more) than that predicted

450   using an analytic dispersion model (Kormann and Meixner, 2001). The discrepancy between the flux

451 footprint model output and our correlation analysis is probably because the model assumes spatial

452 homogeneity in the DMS_{sw} concentrations within the flux footprint. A flux footprint model developed

453 for marine air/sea gas flux measurements would be an invaluable tool for the ocean/atmosphere gas

454 exchange research community.

455 During the SOAP cruise we saw no obvious evidence of a first order biological effect on gas transfer

456 coefficients. From this it could be inferred that surfactants in the dinoflagellate and coccolithophore

457 blooms did not exert a significant effect on water side turbulence. Any modification of the gas transfer

458 velocity vs. wind speed relationship by surfactants or waves during SOAP was masked by other

459 influences upon the variability in gas flux measurements. Minimizing the scatter in gas transfer velocity

460 is critical in order to observe the influence of non-wind speed processes and to draw firm conclusions

461 about their impact upon air/sea gas transfer. The challenge for the gas exchange community is that

462 heterogeneity in seawater DMS concentrations is linked to phytoplankton growth, which likely also

463 determines surfactant effects upon the gas transfer velocity.

464

476

477 **References**

478 Bariteau, L., Helmig, D., Fairall, C. W., Hare, J. E., Hueber, J., and Lang, E. K.: Determination of oceanic ozone deposition
479 by ship-borne eddy covariance flux measurements, Atmos. Meas. Tech., 3, 2, 441-455, 2010.

480   Bell, T. G., De Bruyn, W., Miller, S. D., Ward, B., Christensen, K., and Saltzman, E. S.: Air/sea DMS gas transfer in the
481   North Atlantic: evidence for limited interfacial gas exchange at high wind speed, Atmos. Chem. Phys., 13, 11073-11087,
482   2013.
483   Blomquist, B. W., Fairall, C. W., Huebert, B. J., Kieber, D. J., and Westby, G. R.: DMS sea-air transfer velocity: Direct
484   measurements by eddy covariance and parameterization based on the NOAA/COARE gas transfer model, Geophys. Res.
485   Lett., 33, 7, art. no.-L07601, 10.1029/2006gl025735, 2006.
486   Blomquist, B. W., Huebert, B. J., Fairall, C. W., and Faloona, I. C.: Determining the sea-air flux of dimethylsulfide by eddy
487   correlation using mass spectrometry, Atmos. Meas. Tech., 3, 1, 1-20, 2010.
488   Blomquist, B. W., Fairall, C. W., Huebert, B. J., and Wilson, S. T.: Direct measurement of the oceanic carbon monoxide flux
489   by eddy correlation, Atmos. Meas. Tech., 5, 12, 3069-3075, DOI 10.5194/amt-5-3069-2012, 2012.
490   Coburn, S., Ortega, I., Thalman, R., Blomquist, B., Fairall, C. W., and Volkamer, R.: Measurements of diurnal variations and
491   eddy covariance (EC) fluxes of glyoxal in the tropical marine boundary layer: description of the Fast LED-CE-DOAS
492   instrument, Atmos. Meas. Tech., 7, 10, 3579-3595, 10.5194/amt-7-3579-2014, 2014.
493   Dacey, J. W. H., Wakeham, S. G., and Howes, B. L.: Henry's law constants for dimethylsulfide in fresh water and seawater,
494   Geophys. Res. Lett., 11, 10, 991-994, 1984.
495   Donelan, M. A., Haus, B. K., Plant, W. J., and Troianowski, O.: Modulation of short wind waves by long waves, J. Geophys.
496   Res.-Oceans, 115, C10003, Doi 10.1029/2009jc005794, 2010.
497   Edson, J. B., Hinton, A. A., Prada, K. E., Hare, J. E., and Fairall, C. W.: Direct covariance flux estimates from mobile
498   platforms at sea, Journal of Atmospheric and Oceanic Technology, 15, 2, 547-562, doi: 10.1175/1520-
499   0426(1998)015<0547:DCFEFM>2.0.CO;2, 1998.
500   Elliott, S.: Dependence of DMS global sea-air flux distribution on transfer velocity and concentration field type, Journal of
501   Geophysical Research, 114, G2, doi:10.1029/2008JG000710, 2009.
502   Fairall, C. W., Yang, M., Bariteau, L., Edson, J. B., Helmig, D., McGillis, W., Pezoa, S., Hare, J. E., Huebert, B., and
503   Blomquist, B.: Implementation of the Coupled Ocean-Atmosphere Response Experiment flux algorithm with CO2, dimethyl
504   sulfide, and O3, J. Geophys. Res.-Oceans, 116, C00F09, 10.1029/2010jc006884, 2011.
505   Frew, N. M., Goldman, J. C., Dennett, M. R., and Johnson, A. S.: Impact of phytoplankton-generated surfactants on air-sea
506   gas-exchange, J. Geophys. Res.-Oceans, 95, C3, 3337-3352, Doi 10.1029/Jc095ic03p03337, 1990.
507   Ho, D. T., Wanninkhof, R., Schlosser, P., Ullman, D. S., Hebert, D., and Sullivan, K. F.: Toward a universal relationship
508   between wind speed and gas exchange: Gas transfer velocities measured with ^{3}He/SF$_6$ during the Southern Ocean Gas
509   Exchange Experiment, Journal of Geophysical Research, 116, C4, 10.1029/2010jc006854, 2011.
510   Huebert, B. J., Blomquist, B. W., Hare, J. E., Fairall, C. W., Johnson, J. E., and Bates, T. S.: Measurement of the sea-air
511   DMS flux and transfer velocity using eddy correlation, Geophys. Res. Lett., 31, 23, L23113, 10.1029/2004gl021567, 2004.
512   Huebert, B. J., Blomquist, B. W., Yang, M. X., Archer, S. D., Nightingale, P. D., Yelland, M. J., Stephens, J., Pascal, R. W.,
513   and Moat, B. I.: Linearity of DMS transfer coefficient with both friction velocity and wind speed in the moderate wind speed
514   range, Geophys. Res. Lett., 37, 1, L01605, 10.1029/2009gl041203, 2010.
515   Kim, M. J., Farmer, D. K., and Bertram, T. H.: A controlling role for the air-sea interface in the chemical processing of
516   reactive nitrogen in the coastal marine boundary layer, Proceedings of the National Academy of Sciences, 111, 11, 3943-
517   3948, 10.1073/pnas.1318694111, 2014.
518   Kormann, R., and Meixner, F. X.: An analytical footprint model for non-neutral stratification, Boundary-Layer Meteorology,
519   99, 2, 207-224, 10.1023/a:1018991015119, 2001.
520   Lana, A., Bell, T. G., Simó, R., Vallina, S. M., Ballabrera-Poy, J., Kettle, A. J., Dachs, J., Bopp, L., Saltzman, E. S., Stefels,
521   J., Johnson, J. E., and Liss, P. S.: An updated climatology of surface dimethylsulfide concentrations and emission fluxes in
522   the global ocean, Global Biogeochemical Cycles, 25, 1, art. no.-GB1004, 10.1029/2010gb003850, 2011.
523   Liss, P. S., and Slater, P. G.: Flux of gases across the air-sea interface, Nature, 247, 5438, 181-184, 1974.
524   Marandino, C. A., De Bruyn, W. J., Miller, S. D., Prather, M. J., and Saltzman, E. S.: Oceanic uptake and the global
525   atmospheric acetone budget, Geophys. Res. Lett., 32, 15, art. no.-L15806, 10.1029/2005gl023285, 2005.
526   Marandino, C. A., De Bruyn, W. J., Miller, S. D., and Saltzman, E. S.: Eddy correlation measurements of the air/sea flux of
527   dimethylsulfide over the North Pacific Ocean, Journal of Geophysical Research-Atmospheres, 112, D3, art. no.-D03301,
528   10.1029/2006jd007293, 2007.
529   Marandino, C. A., De Bruyn, W. J., Miller, S. D., and Saltzman, E. S.: DMS air/sea flux and gas transfer coefficients from
530   the North Atlantic summertime coccolithophore bloom, Geophys. Res. Lett., 35, 23, art. no.-L23812, 10.1029/2008gl036370,
531   2008.
532   Marandino, C. A., De Bruyn, W. J., Miller, S. D., and Saltzman, E. S.: Open ocean DMS air/sea fluxes over the eastern South
533   Pacific Ocean, Atmos. Chem. Phys., 9, 2, 345-356, 2009.
534   McGillis, W. R., Edson, J. B., Hare, J. E., and Fairall, C. W.: Direct covariance air-sea CO$_2$ fluxes, J. Geophys. Res.-Oceans,
535   106, C8, 16729-16745, 2001.

536 Miller, S. D., Hristov, T. S., Edson, J. B., and Friehe, C. A.: Platform motion effects on measurements of turbulence and air-
537 sea exchange over the open ocean, Journal of Atmospheric and Oceanic Technology, 25, 9, 1683-1694, Doi
538 10.1175/2008jtecho547.1, 2008.
539 Miller, S. D., Marandino, C., and Saltzman, E. S.: Ship-based measurement of air-sea CO_2 exchange by eddy covariance,
540 Journal of Geophysical Research-Atmospheres, 115, D2, art. no.-D02304, 10.1029/2009jd012193, 2010.
541 Nightingale, P. D., Malin, G., Law, C. S., Watson, A. J., Liss, P. S., Liddicoat, M. I., Boutin, J., and Upstill-Goddard, R. C.:
542 In situ evaluation of air-sea gas exchange parameterizations using novel conservative and volatile tracers, Global
543 Biogeochemical Cycles, 14, 1, 373-387, 2000.
544 Popinet, S., Smith, M., and Stevens, C.: Experimental and numerical study of the turbulence characteristics of airflow around
545 a research vessel, Journal of Atmospheric and Oceanic Technology, 21, 10, 1575-1589, Doi 10.1175/1520-
546 0426(2004)021<1575:Eansot>2.0.Co;2, 2004.
547 Sabine, C. L., Feely, R. A., Gruber, N., Key, R. M., Lee, K., Bullister, J. L., Wanninkhof, R., Wong, C. S., Wallace, D. W.
548 R., Tilbrook, B., Millero, F. J., Peng, T. H., Kozyr, A., Ono, T., and Rios, A. F.: The oceanic sink for anthropogenic CO_2,
549 Science, 305, 5682, 367-371, DOI 10.1126/science.1097403, 2004.
550 Salter, M. E., Upstill-Goddard, R. C., Nightingale, P. D., Archer, S. D., Blomquist, B., Ho, D. T., Huebert, B., Schlosser, P.,
551 and Yang, M.: Impact of an artificial surfactant release on air-sea gas fluxes during Deep Ocean Gas Exchange Experiment
552 II, J. Geophys. Res.-Oceans, 116, C11, 10.1029/2011jc007023, 2011.
553 Saltzman, E. S., King, D. B., Holmen, K., and Leck, C.: Experimental determination of the diffusion coefficient of
554 dimethylsulfide in water, J. Geophys. Res.-Oceans, 98, C9, 16481-16486, 1993.
555 Saltzman, E. S., De Bruyn, W. J., Lawler, M. J., Marandino, C. A., and McCormick, C. A.: A chemical ionization mass
556 spectrometer for continuous underway shipboard analysis of dimethylsulfide in near-surface seawater, Ocean Science, 5, 4,
557 537-546, 2009.
558 Smith, M. J., Ho, D. T., Law, C. S., McGregor, J., Popinet, S., and Schlosser, P.: Uncertainties in gas exchange
559 parameterization during the SAGE dual-tracer experiment, Deep-Sea Res. Part II-Top. Stud. Oceanogr., 58, 6, 869-881, DOI
560 10.1016/j.dsr2.2010.10.025, 2011.
561 Soloviev, A. V.: Coupled renewal model of ocean viscous sublayer, thermal skin effect and interfacial gas transfer velocity,
562 Journal of Marine Systems, 66, 1-4, 19-27, 10.1016/j.jmarsys.2006.03.024, 2007.
563 Soloviev, A. V., Donelan, M., Graber, H., Haus, B., and Schlüssel, P.: An approach to estimation of near-surface turbulence
564 and CO_2 transfer velocity from remote sensing data, Journal of Marine Systems, 66, 1-4, 182-194,
565 10.1016/j.jmarsys.2006.03.023, 2007.
566 Sweeney, C., Gloor, E., Jacobson, A. R., Key, R. M., McKinley, G., Sarmiento, J. L., and Wanninkhof, R.: Constraining
567 global air-sea gas exchange for CO_2 with recent bomb ^{14}C measurements, Global Biogeochemical Cycles, 21, 2, art. no.-
568 GB2015, 10.1029/2006gb002784, 2007.
569 Woolf, D. K.: Bubbles and their role in gas exchange, in: The Sea Surface and Global Change, edited by: Liss, P. S., and
570 Duce, R. A., Cambridge University Press, Cambridge, 173-205, 1997.
571 Yang, M., Blomquist, B. W., and Huebert, B. J.: Constraining the concentration of the hydroxyl radical in a stratocumulus-
572 topped marine boundary layer from sea-to-air eddy covariance flux measurements of dimethylsulfide, Atmos. Chem. Phys.,
573 9, 23, 9225-9236, 2009.
574 Yang, M., Blomquist, B. W., Fairall, C. W., Archer, S. D., and Huebert, B. J.: Air-sea exchange of dimethylsulfide in the
575 Southern Ocean: Measurements from SO GasEx compared to temperate and tropical regions, J. Geophys. Res.-Oceans, 116,
576 10.1029/2010jc006526, 2011.
577 Yang, M., Beale, R., Smyth, T., and Blomquist, B.: Measurements of OVOC fluxes by eddy covariance using a proton-
578 transfer-reaction mass spectrometer - method development at a coastal site, Atmos. Chem. Phys., 13, 13, 6165-6184, DOI
579 10.5194/acp-13-6165-2013, 2013.
580
581